MoS_2 saturable absorber for single frequency oscillation of highly Yb-doped fiber laser

Baole Lu (陆宝乐)[1,2,3,*], Limei Yuan (原莉梅)[1,2,3], Xinyuan Qi (齐新元)[4], Lei Hou (侯 磊)[1,2,3], Bo Sun (孙 博)[1,2,3], Pan Fu (付 盼)[1,2,3], and Jintao Bai (白晋涛)[1,2,3,4]

[1]*National Key Laboratory of Photoelectric Technology and Functional Materials (Culture Base), Institute of Photonics and Photonics-Technology, Northwest University, Xi'an 710069, China*

[2]*Shaanxi Engineering Technology Research Center for Solid State Lasers and Application, Xi'an 710069, China*

[3]*Institute of Photonics and Photonics-Technology, Provincial Key Laboratory of Photoelectronic Technology, Northwest University, Xi'an 710069, China*

[4]*School of Physics, Northwest University, Xi'an 710069, China*

**Corresponding author: lubaole1123@163.com*

Received March 28, 2016; accepted May 16, 2016; posted online June 21, 2016

In this Letter, a single-frequency fiber laser using a molybdenum disulfide (MoS_2) thin film as a saturable absorber is demonstrated. We use a short length of highly Yb-doped fiber as the gain medium and a fiber ferrule with MoS_2 film adhered to it by index matching gel (IMG) that acts as the saturable absorber. The saturable absorber can be used to discriminate and select the single longitudinal modes. The maximum output power of the single-frequency fiber laser is 15.3 mW at a pump power of 130 mW and the slope efficiency is 15.3%. The optical signal-to-noise ratio and the laser linewidths are ~60 dB and 5.89 kHz, respectively.

OCIS codes: 140.3510, 140.3570, 160.3380.
doi: 10.3788/COL201614.071404.

Single-frequency (SF) lasers have properties of narrow linewidth, high signal-to-noise ratio (SNR), system compactness, and long operation life. Due to their excellent characteristics, SF lasers have attracted great attention, especially the SF fiber lasers around 1 μm, which have very promising applications in various areas such as coherent telecommunications, optical fiber sensors, laser ranging, as well as coherent beam combination[1–4].

Different kinds of SF lasers have been realized over the years. Most previously presented SF solid-state lasers are based on an intracavity crystal, etalons, and a monolithic nonplanar ring oscillator[5–9]. Although these SF solid-state lasers have stable structures and high efficiency, the linewidths are about the MHz level[7]. Consequently, several new methods have been used to realize narrow linewidth all-fiber lasers in the recent years. Morkel *et al.* demonstrated an SF fiber laser with a maximum output power of over 200 mW and linewidth of less than 7 kHz at 1.95 μm by using the self-developed heavily Tm^{3+}-doped single-mode germanate glass fiber as the active fiber in a ring cavity, and the slope efficiency measured versus the absorbed pump power was 34.8%[10]. Meng *et al.* reported a 40 Hz ultra-narrow linewidth SF fiber laser at 1550 nm with a maximum output power of about 6 mW at 0.37 mW Brillouin pump power and 383 mW 980 nm pump power by employing an erbium-doped fiber as both Brillouin and gain media in a ring cavity[11]. The ring cavity fiber laser exhibits excellent characteristics in the linewidth and in the output stability. Nevertheless, the complicated structure and rather low slope efficiency limit the extensive applications. In addition, the short linear-cavity structures (distributed Bragg reflector (DBR)[12] and distributed feedback (DFB)[13]) are beneficial to SF laser emission for their narrow linewidth and low noise, which are quite difficult to fabricate due to their complicated techniques and expensive costs. For these reasons, a novel type of linear-cavity fiber laser with a doped fiber in a loop mirror filter (LMF) as the saturable absorber (SA) is proposed[14,15]. The cavity design is easy to implement and costs less.

Recently, the emergence of two-dimensional (2D) materials has provided another simple way to achieve the SF laser. Graphene, a type of zero bandgap 2D nanomaterial with a broadband saturable absorption and a low saturable absorbing threshold, is accepted as a prominent material for the fabrication of high-performance SAs[16,17]. Muhammad *et al.* employed a multilayer graphene as the SA in a ring cavity, and then successfully generated a conventional wavelength band fiber laser with a tunable single-longitudinal-mode laser output[18]. Zhou *et al.* proposed and demonstrated a dual-wavelength SF fiber laser based on a graphene SA and wave shape. The linewidths and the side-mode suppression ratios of the two wavelengths are both less than 7.3 kHz and larger than 50 dB, respectively[19]. In addition, Chen *et al.* experimentally demonstrated a single-longitudinal mode erbium-doped fiber laser with a maximum output power of 23 mW at 1 W 1480 nm pump power and linewidth of less than 10 kHz by using a topolopical insulator (TI) Bi_2Te_3 as the SA[20]. Very recently, MoS_2 was a typical transition metal dichalcogenide in which hexagonal layers of molybdenum atoms were sandwiched between two layers of chalcogen atom (S). MoS_2 has a natural direct bandgap, which is adjustable according to the number of layers. Wang *et al.* reported that the MoS_2 nanosheets have a better saturable

absorption response than that of graphene at 800 nm[21]. Zhang *et al.* investigated the nonlinear optical property of few-layered MoS_2 from the visible to the near-infrared band and demonstrated the broadband saturable absorption at the 400, 800, and 1060 nm wavebands[22]. These studies indicate that the few-layer MoS_2 is a promising candidate for a broadband SA.

In this Letter, we present a 1064 nm SF fiber laser with a linear cavity in which three polarization controllers (PCs), an MoS_2 film embedded in a fiber loop mirror acting as an SA, are employed[23]. The structure of our configuration combines the advantages of LMF and MoS_2, which is simple and compact. The MoS_2 can be used in a wide spectral operating range for different lasers and will be easily popularized in the future. We obtained the maximum output power of the SF laser as 15.3 mW at a slope efficiency of 15.3%. The SNR is ~60 dB and the corresponding linewidth is 5.89 kHz. To the best of our knowledge, this is the first demonstration of a 5.89 kHz 1064 nm SF laser based on LMF by incorporating MoS_2.

The MoS_2 was prepared by the chemical vapor deposition (CVD) method in our experiment. In a typical growth, the MoS_3 (99.99%, 0.05 g) and sulfur (S) particles (99.999%, 0.1 g) were used as the reaction sources. A homemade three-temperature zone CVD furnace equipped with a four inch quartz tube was used as the reactor. The MoS_2 film was grown on various substratesthat were placed near the pumping end, while sulfur was placed near the gas vent. The MoO_3 was loaded in a quartz crucible and placed in the center of the furnace. The system's vacuum was pumped to 1 Pa and 500 standard cubic centimeter per minute (SCCM), and the Ar gas was used as the protection gas. The S particles, MoS_3, and sapphire wafer were heated up to 180°C, 750°C, and 650°C within 40 min, respectively, and the temperatures were kept for 15 min for the growth of the MoS_2 film. For the transfer of the MoS_2 film, the poly (methyl methacrylate) (PMMA) solution (anisole, 5% content) was spun to the surface of the MoS_2 to protect the film. A 5 mol/L NaOH solution was used for the etching process. After drying 2 h (at 60°C) in the furnace, the MoS_2 film was separated from the sapphire substrate mechanically with an ultrathin PET tape[24]. Such a large area of MoS_2 film could be used as an SA directly.

The Raman spectrum of the MoS_2 film is shown in Fig. 1(a). The sample exhibits two characteristic peaks that correspond to the in-plane vibration of Mo and S atoms (E^1_{2g} mode) at 383.5 cm^{-1} and the out-of-plane vibration of S atoms (Ag^1) at 407.8 cm^{-1}, respectively. The separation of the two peaks depends on the layer thickness of MoS_2[25]. In our experiment, a frequency difference of ~24.3 cm^{-1} is calculated, which corresponds to 4–5 layers of MoS_2. Besides, the thickness of a single layer of MoS_2 is about 0.65 nm, then the thickness of MoS_2 SA that used in our experiment is about 2.6–3.25 nm. The transmission spectrum of the multilayer MoS_2 is measured by the Macroscopic Angle resolution spectrum system, as shown in Fig. 1(b). The transmittance of the MoS_2 is

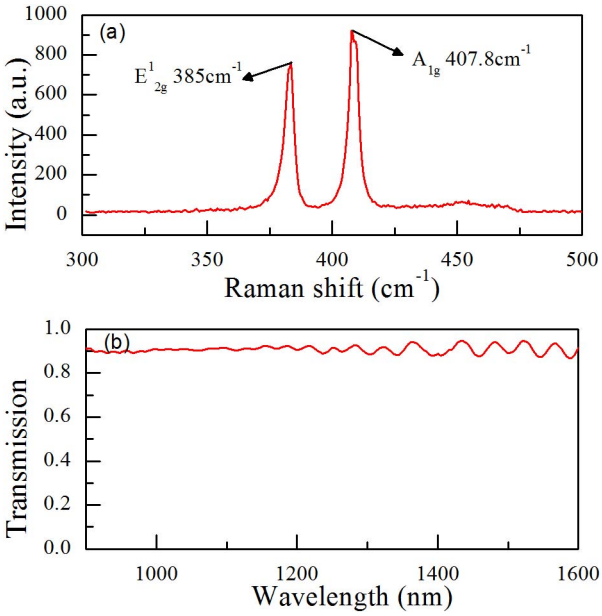

Fig. 1. (a) Raman spectrum of the MoS_2 film. (b) The transmission spectrum of the MoS_2 film.

about 91% at the wavelength near 1064 nm (the absorption is about 9%).

The experimental schematic of the SF all-fiber laser is shown in Fig. 2, which is similar to that in Ref. [15]. A continuous wave laser at 975 nm was imported by WDM1 (980/1060 nm, 1×2) into a narrow-band fiber Bragg grating (FBG, with reflectivity of 60% at 1064 nm). A 16 cm-long single-mode single-clad ytterbium-doped fiber (INO Yb 501) was used as the gain medium. The linear cavity was composed of the FBG and the LMF, and the optical path length of the cavity was less than 1 m (exclusive of the LMF). As was known to all, the spatial hole burning (SHB) effect could not be avoided, which was generated by the nonlinear wave mixing of the two counter-propagating waves and caused the multiple longitudinal mode oscillation[26]. So the PC2 was introduced to destroy the interference pattern of the two counter-propagating waves and suppress the SHB effect in the linear cavity. The LMF acting as a narrowband filter suppressed the other unwanted longitudinal mode oscillations, which consisted of a fiber loop mirror with a 3 dB coupler, an SA (an MoS_2 film inserted in the adapter), and two PCs.

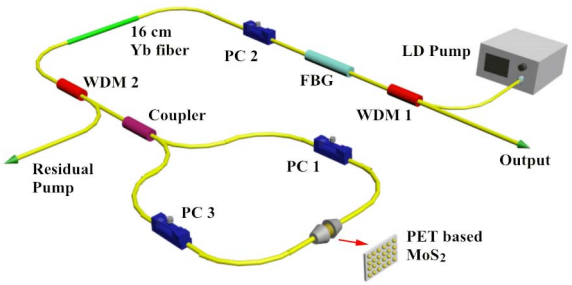

Fig. 2. Experimental setup of the SF fiber laser based on the LMF. WDM: wavelength division multiplexer.

The LMF without the SA film was a traditional interferometer with a 3 dB coupler, which acted as a total reflection mirror[27]. In the reflecting mirror, the entering optical field was split into two counter-propagating parts by the 3 dB coupler, and the nonlinear phase shifts were equal for both waves, resulting in no relative phase difference between them, so the light would be reflected totally[23,28]. When the SA film was employed in the fiber loop mirror, the mirror could also efficiently suppress the multimode. The LMF played a key role in the mode selection and the linewidth narrowing. By better adjusting the polarization state of the light, adding the PC3 in the LMF, a narrower and more stable SF oscillation was achieved.

One of the key components in the experiment setup was the MoS_2 film. The MoS_2 film in the Sagnac fiber loop mirror acted as a filter that prevented other modes from lasing and confined the system to SLM operation. The MoS_2 was used to suppress the multi-longitudinal mode and noise in a fiber laser. For the low-intensity light incident, photons were highly absorbed and the electrons in the valence band were excited to the conduction band of the SA material. For the high-intensity light incident, some photons were not absorbed due to the occupation of electrons in the conduction band, which were excited by the photons from the low-intensity light. Therefore, the light of low energy was absorbed, and high energy light passed without loss[18,19], which could be used to effectively narrow the linewidth in a laser. In terms of the absorption, the SA revealed only an intensity-dependent transmission or loss[29]. Furthermore, unnecessary thickness of the MoS_2 film must be avoided, since the higher thickness contributes to higher losses. The WDM2 (980/1060 nm, 1×2) was employed to output the residual pump beam. The output laser from WDM1 was scanned by a Fabry–Perot (F–P) interferometer (Thorlabs, SA201 with a free spectral range (FSR) of 10 GHz and a resolution of 67 MHz) and analyzed by an oscilloscope (OSC, Agilent Infiniium 9000, with a resolution of 0.02 nm). The spectrum of the SF fiber laser was recorded by an optical spectrum analyzer (OSA, YOKOGAWA AQ6370B with a resolution of 0.02 nm). To monitor the stability of the output laser, a power meter was used.

In the experiment, we generated a 1064 nm laser by increasing the pump power to an appropriate value. The multi-longitudinal modes were observed without adjusting the three PCs [Fig. 3(a)]. The black sawtooth wave is the F–P ramp voltage, which approximately provides two FSRs. The red curve is the wave signal of the laser passing through F–P interferometer in the FSR voltage. According to the design principle and the structure of the resonant cavity, we adjust PC1 and PC3 to optimize the loop mirror reflection. Then the number of longitudinal modes decreases drastically; only a few modes operated in one FSR [Fig. 3(b)]. This phenomenon shows that the MoS_2 SA has worked. So only when the intensity of the longitudinal mode is high, would the mode transmit through the SA with very low loss and vice versa. Except for the strong signal peak, there is a weak envelope in the

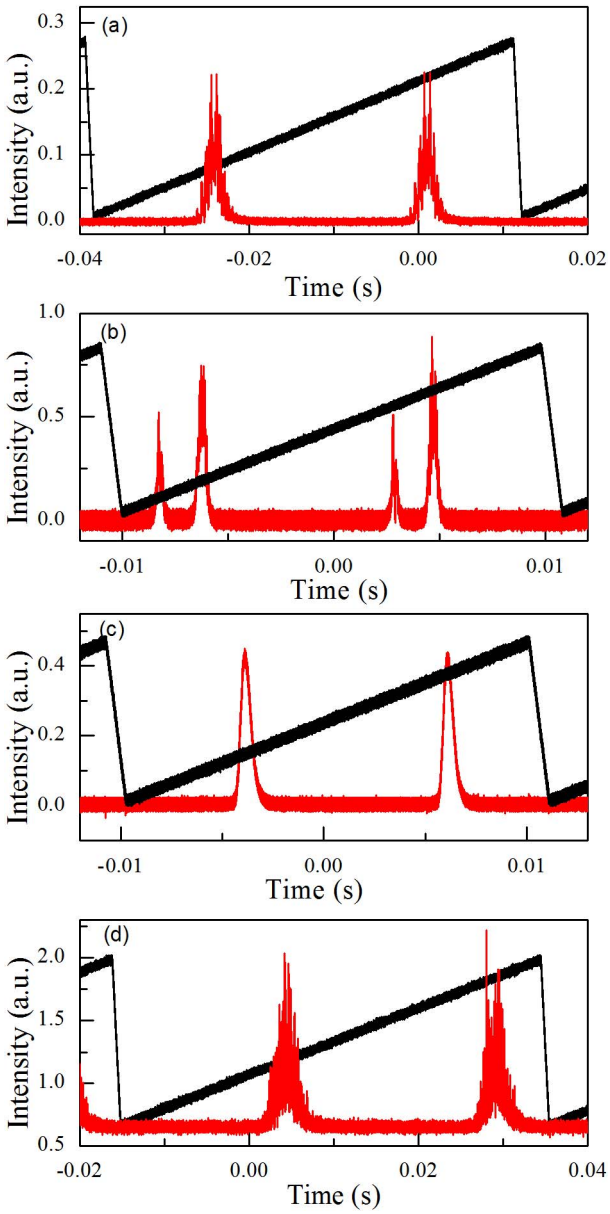

Fig. 3. Longitudinal mode oscillations over one FSR scanned by an F–P interferometer. (a) Multi-longitudinal mode oscillation without PC. (b) Longitudinal mode oscillation with PC1 and PC3. (c) Single longitudinal mode oscillation with PC2. (d) Multi-longitudinal mode oscillation without the MoS_2 film.

FSR, as shown in Fig. 3(b). What is more, the boundaries of the two envelopes are jagged instead of smooth, which shows that one envelope does not only contain one longitudinal mode. That may be caused by the influence of the SHB, and the side modes near the center frequency would not be well suppressed. So PC2 was adopted to adjust the wave polarization to restrain the SHB effect. When the pump power was increased to 130 mW, we obtained the maximum output power for the 15.3 mW SF laser. A standard graph of the single longitudinal mode oscillation spectrum information that was observed is shown in Fig. 3(c). There is only one longitudinal mode present in an FSR (10 GHz) of the F–P interferometer, which

confirms that the SF oscillation is attained. The SF oscillation is very stable. Nevertheless, the multi-longitudinal mode oscillations and mode hopping appeared when the pump power was increased more than 130 mW, as shown in Fig. 3(b). That can be attributed to the SHB effect induced by the high light intensity in the cavity, which cannot be suppressed by the adjustment of PC2 and the LMF. In order to further verify the role of the MoS_2 film, we got rid of the MoS_2 film in the LMF and other parts stayed the same, simply breaking the LMF and splicing the two ports of the 3 dB coupler directly. Then we repeated the same experiment operation as before; the irregular multimode oscillations were observed as shown in Fig. 3(d). No matter how we adjusted the three PCs, there was no SF signal all the time, and only the multi-longitudinal mode oscillations could be observed through the OSC. This phenomenon demonstrated the crucial role of MoS_2 as the SA in the experiment.

Figure 4(a) illustrates the emission spectra of the SF laser with the MoS_2 at room temperature. The central wavelength is about 1063.88 nm at the output power of 15.3 mW and there is no other emission peak. The SNR is ~60 dB. From the Fig. 4(b), we can see that when the pump power is above the threshold, the laser output power enhances linearly. The lasing threshold is around 21 mW. The maximum output power of the SF laser reaches about 15.3 mW when the pump power is 130 mW. The slope efficiency is 15.3%. After the fiber laser works for a period, the output power of the laser becomes stable obviously. The stability curves of the output power at 12.9 mW and wavelength at 1063.88 nm are both plotted in Fig. 4(c). The power instability of $< \pm 2.7\%$ of the average power during 1 h is observed [blue triangle line in Fig. 4(c)]. The wavelength instability of the center wavelength is less than 0.3% [red square line in Fig. 4(c)]. The instabilities of the output power and wavelength are caused by small fluctuations in the pump laser power and small changes of ambient temperature.

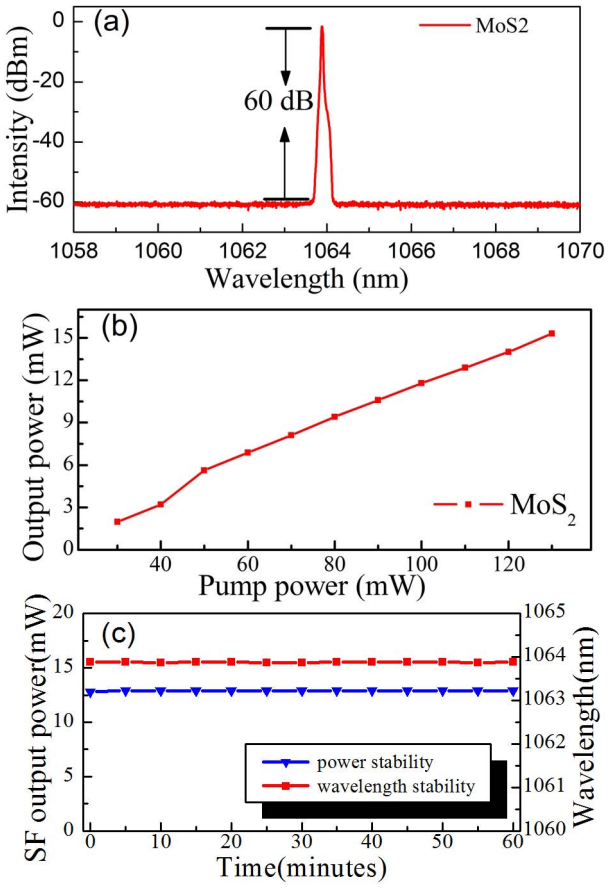

Fig. 4. (a) Emission spectrum of the SF laser with the MoS_2. (b) The output power versus pump power of the SF laser. (c) The power and wavelength stabilities of the fiber laser for 1 h.

To further investigate the phase noise characteristics, the linewidth of the SF fiber laser was measured by the delayed self-heterodyne method using a 30 km fiber delay[30]. The SF laser beam was split into two beams by a 3 dB coupler. One beam as the reference light was delayed by a 30 km single-mode delay fiber, and the other beam as the signal light was through an acousto-optic modulator with a carrier frequency of 150 MHz (Gooch S-M150-0.4C2 G-3-F2 S). Next, the two beams were recombined by the 3 dB coupler to obtain the beat frequency spectrum signal and went through the photoelectric detector with a bandwidth of 2 GHz (THORLABS DET01CFC). Finally, the signal was analyzed by a radio frequency spectrum analyzer (KEYSIGHT N9320B), which set the resolution bandwidth of 1 kHz. Figure 5 shows the result of the measurement with the MoS_2 SA. From the heterodyne signal, we take 3 dB down from the maximum value to estimate its bandwidth, which is less than 12 kHz. The laser linewidth is equal to the half-width of the heterodyne signal, which is 5.89 kHz with the MoS_2 SA (in Fig. 5).

In conclusion, we study an SF 1064 nm laser with an all-fiber linear cavity. The ytterbium-doped fiber and the MoS_2 film are employed as the gain medium and the SA in the LMF, respectively. Three PCs are used to adjust the state of the light polarization. The maximum output power of the SF fiber laser reaches 15.3 mW when the pump power is 130 mW. The slope efficiency and the SNR of the SF laser oscillation are 15.3% and ~60 dB, respectively. The laser linewidth is 5.89 kHz. The results

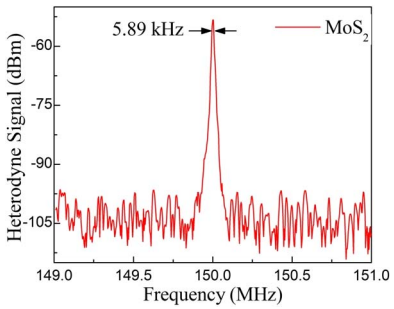

Fig. 5. Line shape of the heterodyne signal measured with a 30 km fiber delay.

demonstrate that MoS_2 films have strong characteristics of SA and can act as promising filters for SF laser systems.

This work was supported by the National Natural Science Foundation of China (No. 61475125), the Natural Science Foundation of Shaanxi Province, China (No. 2016JM6083), and the Science Foundation of Northwest University (No. 15NW07).

References

1. J. Geng, C. Spiegelberg, and S. Jiang, IEEE Photon. Technol. Lett. **17**, 1827 (2005).
2. G. J. Ray, T. N. Anderson, J. A. Caton, R. P. Lucht, and T. Walther, Opt. Lett. **26**, 1870 (2001).
3. J. G. Williams, S. G. Turyshev, and D. H. Boggs, Phys. Rev. Lett. **93**, 261101 (2004).
4. R. Su, P. Zhou, X. Wang, H. Zhang, and X. Xu, Opt. Lett. **37**, 3978 (2012).
5. H. Lu, J. Su, Y. Zheng, and K. Peng, Opt. Lett. **39**, 1117 (2014).
6. L. Wang, C. Gao, M. Gao, L. Liu, and F. Yue, Appl. Opt. **52**, 1272 (2013).
7. B. Q. Yao, X. Yu, X. L. Liu, X. M. Duan, Y. L. Ju, and Y. Z. Wang, Opt. Express **21**, 8916 (2013).
8. T. Lu, J. Wang, X. Zhu, R. Zhu, H. Zang, and W. Chen, Chin. Opt. Lett. **11**, 36 (2013).
9. Y. Ju, W. Liu, B. Yao, T. Dai, J. Wu, J. Yuan, J. Wang, X. Duan, and Y. Wang, Chin. Opt. Lett. **13**, 111403 (2015).
10. X. He, S. Xu, C. Li, C. Yang, Q. Yang, S. Mo, D. Chen, and Z. Yang, Opt. Express **21**, 20800 (2013).
11. M. Chen, Z. Meng, Y. Zhang, J. Wang, and W. Chen, IEEE Photon. J. **7**, 1 (2015).
12. Z. Feng, S. Mo, S. Xu, X. Huang, Z. Zhong, C. Yang, C. Li, W. Zhang, D. Chen, and Z. Yang, Appl. Phys. E. **6**, 0527101 (2013).
13. J. Shi, S.-U. Alam, and M. Ibsen, in *Conference on Lasers and Electro-Optics (CLEO)* (2012).
14. S. Huang, Y. Feng, J. Dong, A. Shirakawa, M. Musha, and K. Ueda, Laser. Phys. Lett. **2**, 498 (2005).
15. B.-L. Lu, S.-H. Huang, M.-J. Yin, H.-W. Chen, Z.-Y. Ren, and J.-T. Bai, Chin. Phys. Lett. **32**, 044201 (2015).
16. M. Liu, X. W. Zheng, Y. L. Qi, H. Liu, A. P. Luo, Z. C. Luo, W. C. Xu, C. J. Zhao, and H. Zhang, Opt. Express **22**, 22841 (2014).
17. J. Zhou, A. Luo, Z. Luo, X. Wang, X. Feng, and B. Guan, Photon. Res. **3**, A21 (2015).
18. F. D. Muhammad, M. Z. Zulkifli, A. A. Latif, S. W. Harun, and H. Ahmad, IEEE Photon. J. **4**, 467 (2012).
19. J. Zhou, A. Luo, Z. Luo, Z. H. Luo, X. Wang, X. Feng, and B. Guan, in *Asia Communications and Photonics Conference*, ATh3A.76 (2014).
20. S. Chen, Q. Wang, C. Zhao, Y. Li, H. Zhang, and S. Wen, J. Lightwave Technol. **32**, 4438 (2014).
21. H. Zhang, S. B. Lu, J. Zheng, J. Du, S. C. Wen, D. Y. Tang, and K. P. Loh, Opt. Express **22**, 7249 (2014).
22. S. Wang, H. Yu, H. Zhang, A. Wang, M. Zhao, Y. Chen, L. Mei, and J. Wang, Adv. Mater. **26**, 3538 (2014).
23. S. A. Havstad, B. Fischer, A. E. Willner, and M. G. Wickham, Opt. Lett. **24**, 1466 (1999).
24. H. Xia, H. Li, C. Lan, C. Li, X. Zhang, S. Zhang, and Y. Liu, Opt. Express **22**, 17341 (2014).
25. H. Li, Q. Zhang, C. C. R. Yap, B. K. Tay, T. H. T. Edwin, A. Olivier, and D. Baillargeat, Adv. Funct. Mater. **22**, 1385 (2012).
26. M. Horowitz, R. Daisy, B. Fischer, and J. L. Zyskind, Opt. Lett. **19**, 1406 (1994).
27. M. Yin, S. Huang, B. Lu, H. Chen, Z. Ren, and J. Bai, Appl. Opt. **52**, 6799 (2015).
28. V. Haan, R. Santbergen, M. Tijssen, and M. Zeman, Appl. Opt. **50**, 5674 (2011).
29. L. Zhang, L. Zhan, M. Qin, Z. Zou, Z. Wang, and J. Liu, J. Opt. Soc. Am. B **32**, 1113 (2015).
30. L. Richter, H. Mandelberg, M. Kruger, and P. McGrath, IEEE J. Quantum. Electron. **22**, 2070 (1986).